Eur. Phys. J. C 5, 1–17 (1998)
DOI 10.1007/s100529800894

THE EUROPEAN PHYSICAL JOURNAL C
© Springer-Verlag 1998

Determination of the production rate of D^{*0} mesons and of the ratio $V/(V+P)$ in $\mathrm{Z}^0 \to \mathrm{c\bar{c}}$ decays

OPAL Collaboration

K. Ackerstaff[8], G. Alexander[23], J. Allison[16], N. Altekamp[5], K.J. Anderson[9], S. Anderson[12], S. Arcelli[2], S. Asai[24], S.F. Ashby[1], D. Axen[29], G. Azuelos[18,a], A.H. Ball[17], E. Barberio[8], R.J. Barlow[16], R. Bartoldus[3], J.R. Batley[5], S. Baumann[3], J. Bechtluft[14], T. Behnke[8], K.W. Bell[20], G. Bella[23], S. Bentvelsen[8], S. Bethke[14], S. Betts[15], O. Biebel[14], A. Biguzzi[5], S.D. Bird[16], V. Blobel[27], I.J. Bloodworth[1], M. Bobinski[10], P. Bock[11], D. Bonacorsi[2], M. Boutemeur[34], S. Braibant[8], L. Brigliadori[2], R.M. Brown[20], H.J. Burckhart[8], C. Burgard[8], R. Bürgin[10], P. Capiluppi[2], R.K. Carnegie[6], A.A. Carter[13], J.R. Carter[5], C.Y. Chang[17], D.G. Charlton[1,b], D. Chrisman[4], P.E.L. Clarke[15], I. Cohen[23], J.E. Conboy[15], O.C. Cooke[8], C. Couyoumtzelis[13], R.L. Coxe[9], M. Cuffiani[2], S. Dado[22], C. Dallapiccola[17], G.M. Dallavalle[2], R. Davis[30], S. De Jong[12], L.A. del Pozo[4], A. de Roeck[8], K. Desch[3], B. Dienes[33,d], M.S. Dixit[7], M. Doucet[18], E. Duchovni[26], G. Duckeck[34], I.P. Duerdoth[16], D. Eatough[16], P.G. Estabrooks[6], E. Etzion[23], H.G. Evans[9], M. Evans[13], F. Fabbri[2], A. Fanfani[2], M. Fanti[2], A.A. Faust[30], L. Feld[8], F. Fiedler[27], M. Fierro[2], H.M. Fischer[3], I. Fleck[8], R. Folman[26], D.G. Fong[17], M. Foucher[17], A. Fürtjes[8], D.I. Futyan[16], P. Gagnon[7], J.W. Gary[4], J. Gascon[18], S.M. Gascon-Shotkin[17], N.I. Geddes[20], C. Geich-Gimbel[3], T. Geralis[20], G. Giacomelli[2], P. Giacomelli[4], R. Giacomelli[2], V. Gibson[5], W.R. Gibson[13], D.M. Gingrich[30,a], D. Glenzinski[9], J. Goldberg[22], M.J. Goodrick[5], W. Gorn[4], C. Grandi[2], E. Gross[26], J. Grunhaus[23], M. Gruwé[27], C. Hajdu[32], G.G. Hanson[12], M. Hansroul[8], M. Hapke[13], C.K. Hargrove[7], P.A. Hart[9], C. Hartmann[3], M. Hauschild[8], C.M. Hawkes[5], R. Hawkings[27], R.J. Hemingway[6], M. Herndon[17], G. Herten[10], R.D. Heuer[8], M.D. Hildreth[8], J.C. Hill[5], S.J. Hillier[1], P.R. Hobson[25], A. Hocker[9], R.J. Homer[1], A.K. Honma[28,a], D. Horváth[32,c], K.R. Hossain[30], R. Howard[29], P. Hüntemeyer[27], D.E. Hutchcroft[5], P. Igo-Kemenes[11], D.C. Imrie[25], K. Ishii[24], A. Jawahery[17], P.W. Jeffreys[20], H. Jeremie[18], M. Jimack[1], A. Joly[18], C.R. Jones[5], M. Jones[6], U. Jost[11], P. Jovanovic[1], T.R. Junk[8], J. Kanzaki[24], D. Karlen[6], V. Kartvelishvili[16], K. Kawagoe[24], T. Kawamoto[24], P.I. Kayal[30], R.K. Keeler[28], R.G. Kellogg[17], B.W. Kennedy[20], J. Kirk[29], A. Klier[26], S. Kluth[8], T. Kobayashi[24], M. Kobel[10], D.S. Koetke[6], T.P. Kokott[3], M. Kolrep[10], S. Komamiya[24], R.V. Kowalewski[28], T. Kress[11], P. Krieger[6], J. von Krogh[11], P. Kyberd[13], G.D. Lafferty[16], R. Lahmann[17], W.P. Lai[19], D. Lanske[14], J. Lauber[15], S.R. Lautenschlager[31], I. Lawson[28], J.G. Layter[4], D. Lazic[22], A.M. Lee[31], E. Lefebvre[18], D. Lellouch[26], J. Letts[12], L. Levinson[26], B. List[8], S.L. Lloyd[13], F.K. Loebinger[16], G.D. Long[28], M.J. Losty[7], J. Ludwig[10], D. Lui[12], A. Macchiolo[2], A. Macpherson[30], M. Mannelli[8], S. Marcellini[2], C. Markopoulos[13], C. Markus[3], A.J. Martin[13], J.P. Martin[18], G. Martinez[17], T. Mashimo[24], P. Mättig[26], W.J. McDonald[30], J. McKenna[29], E.A. Mckigney[15], T.J. McMahon[1], R.A. McPherson[28], F. Meijers[8], S. Menke[3], F.S. Merritt[9], H. Mes[7], J. Meyer[27], A. Michelini[2], S. Mihara[24], G. Mikenberg[26], D.J. Miller[15], A. Mincer[22,e], R. Mir[26], W. Mohr[10], A. Montanari[2], T. Mori[24], S. Mihara[24], K. Nagai[26], I. Nakamura[24], H.A. Neal[12], B. Nellen[3], R. Nisius[8], S.W. O'Neale[1], F.G. Oakham[7], F. Odorici[2], H.O. Ogren[12], A. Oh[27], N.J. Oldershaw[16], M.J. Oreglia[9], S. Orito[24], J. Pálinkás[33,d], G. Pásztor[32], J.R. Pater[16], G.N. Patrick[20], J. Patt[10], R. Perez-Ochoa[8], S. Petzold[27], P. Pfeifenschneider[14], J.E. Pilcher[9], J. Pinfold[30], D.E. Plane[8], P. Poffenberger[28], B. Poli[2], A. Posthaus[3], C. Rembser[8], S. Robertson[28], S.A. Robins[22], N. Rodning[30], J.M. Roney[28], A. Rooke[15], A.M. Rossi[2], P. Routenburg[30], Y. Rozen[22], K. Runge[10], O. Runolfsson[8], U. Ruppel[14], D.R. Rust[12], K. Sachs[10], T. Saeki[24], O. Sahr[34], W.M. Sang[25], E.K.G. Sarkisyan[23], C. Sbarra[29], A.D. Schaile[34], O. Schaile[34], F. Scharf[3], P. Scharff-Hansen[8], J. Schieck[11], P. Schleper[11], B. Schmitt[8], S. Schmitt[11], A. Schöning[8], M. Schröder[8], M. Schumacher[3], C. Schwick[8], W.G. Scott[20], T.G. Shears[8], B.C. Shen[4], C.H. Shepherd-Themistocleous[8], P. Sherwood[15], G.P. Siroli[2], A. Sittler[27], A. Skillman[15], A. Skuja[17], A.M. Smith[8], G.A. Snow[17], R. Sobie[28], S. Söldner-Rembold[10], R.W. Springer[30], M. Sproston[20], K. Stephens[16], J. Steuerer[27], B. Stockhausen[3], K. Stoll[10], D. Strom[19], R. Ströhmer[34], P. Szymanski[20], R. Tafirout[18], S.D. Talbot[1], P. Taras[18], S. Tarem[22], R. Teuscher[8], M. Thiergen[10], M.A. Thomson[8], E. von Törne[3], E. Torrence[8], S. Towers[6], I. Trigger[18], Z. Trócsányi[33], E. Tsur[23], A.S. Turcot[9], M.F. Turner-Watson[8], I. Ueda[24], P. Utzat[11], R. Van Kooten[12], P. Vannerem[10], M. Verzocchi[10], P. Vikas[18], E.H. Vokurka[16], H. Voss[3], F. Wäckerle[10], A. Wagner[27], C.P. Ward[5], D.R. Ward[5], P.M. Watkins[1], A.T. Watson[1], N.K. Watson[1], P.S. Wells[8], N. Wermes[3], J.S. White[28], G.W. Wilson[27], J.A. Wilson[1], T.R. Wyatt[16], S. Yamashita[24], G. Yekutieli[26], V. Zacek[18], D. Zer-Zion[8]

[1] School of Physics and Astronomy, University of Birmingham, Birmingham B15 2TT, UK
[2] Dipartimento di Fisica dell' Università di Bologna and INFN, I-40126 Bologna, Italy

[3] Physikalisches Institut, Universität Bonn, D-53115 Bonn, Germany
[4] Department of Physics, University of California, Riverside CA 92521, USA
[5] Cavendish Laboratory, Cambridge CB3 0HE, UK
[6] Ottawa-Carleton Institute for Physics, Department of Physics, Carleton University, Ottawa, Ontario K1S 5B6, Canada
[7] Centre for Research in Particle Physics, Carleton University, Ottawa, Ontario K1S 5B6, Canada
[8] CERN, European Organisation for Particle Physics, CH-1211 Geneva 23, Switzerland
[9] Enrico Fermi Institute and Department of Physics, University of Chicago, Chicago IL 60637, USA
[10] Fakultät für Physik, Albert Ludwigs Universität, D-79104 Freiburg, Germany
[11] Physikalisches Institut, Universität Heidelberg, D-69120 Heidelberg, Germany
[12] Indiana University, Department of Physics, Swain Hall West 117, Bloomington IN 47405, USA
[13] Queen Mary and Westfield College, University of London, London E1 4NS, UK
[14] Technische Hochschule Aachen, III Physikalisches Institut, Sommerfeldstrasse 26-28, D-52056 Aachen, Germany
[15] University College London, London WC1E 6BT, UK
[16] Department of Physics, Schuster Laboratory, The University, Manchester M13 9PL, UK
[17] Department of Physics, University of Maryland, College Park, MD 20742, USA
[18] Laboratoire de Physique Nucléaire, Université de Montréal, Montréal, Quebec H3C 3J7, Canada
[19] University of Oregon, Department of Physics, Eugene OR 97403, USA
[20] Rutherford Appleton Laboratory, Chilton, Didcot, Oxfordshire OX11 0QX, UK
[22] Department of Physics, Technion-Israel Institute of Technology, Haifa 32000, Israel
[23] Department of Physics and Astronomy, Tel Aviv University, Tel Aviv 69978, Israel
[24] International Centre for Elementary Particle Physics and Department of Physics, University of Tokyo, Tokyo 113, and Kobe University, Kobe 657, Japan
[25] Institute of Physical and Environmental Sciences, Brunel University, Uxbridge, Middlesex UB8 3PH, UK
[26] Particle Physics Department, Weizmann Institute of Science, Rehovot 76100, Israel
[27] Universität Hamburg/DESY, II Institut für Experimental Physik, Notkestrasse 85, D-22607 Hamburg, Germany
[28] University of Victoria, Department of Physics, P O Box 3055, Victoria BC V8W 3P6, Canada
[29] University of British Columbia, Department of Physics, Vancouver BC V6T 1Z1, Canada
[30] University of Alberta, Department of Physics, Edmonton AB T6G 2J1, Canada
[31] Duke University, Dept of Physics, Durham, NC 27708-0305, USA
[32] Research Institute for Particle and Nuclear Physics, H-1525 Budapest, P O Box 49, Hungary
[33] Institute of Nuclear Research, H-4001 Debrecen, P O Box 51, Hungary
[34] Ludwigs-Maximilians-Universität München, Sektion Physik, Am Coulombwall 1, D-85748 Garching, Germany

Received: 12 January / Published online: 13 July 1998

Abstract. In e^+e^- collisions at centre-of-mass energies around 91 GeV, D^{*0} mesons have been reconstructed using data collected with the OPAL detector at LEP. The hadronisation fraction has been measured to be

$$f(c \to D^{*0}) = 0.218 \pm 0.054 \pm 0.045 \pm 0.007\,,$$

where the errors correspond to the statistical and systematic errors specific to this analysis, and to systematic uncertainties from externally measured branching fractions, respectively. Together with previous OPAL measurements of the hadronisation fractions of other charmed mesons, this value is used to investigate the relative production of observed vector and pseudoscalar charmed mesons in $Z^0 \to c\bar{c}$ decays. The production ratio is determined to be

$$P_V^{\rm eff} = V/(V+P) = 0.57 \pm 0.05\ .$$

The relative primary production of vector and pseudoscalar mesons, $P_V^{\rm prim}$, is studied in the context of the production and decay of orbitally excited charmed resonances. The first measurement of the inclusive D_s^{*+} production rate in hadronic Z^0 decays is presented.

1 Introduction

A meson with no orbital angular momentum can be a vector (V) state with spin 1 or a pseudoscalar (P) state with spin 0. Their relative production $P_V = V/(V+P)$ is sensitive to non-perturbative effects in the hadronisation process and cannot be calculated exactly. However, several models [1] have been proposed which predict this ratio. A simple spin counting picture, where the abundance of a

[a] and at TRIUMF, Vancouver, Canada V6T 2A3
[b] and Royal Society University Research Fellow
[c] and Institute of Nuclear Research, Debrecen, Hungary
[d] and Department of Experimental Physics, Lajos Kossuth University, Debrecen, Hungary
[e] and Department of Physics, New York University, NY 1003, USA

particular state is proportional to its number of spin degrees of freedom[1], predicts a value of P_V=0.75 when only vector and pseudoscalar meson production are considered. More sophisticated models take into account the mass difference between vector and pseudoscalar mesons, as well as the masses of the constituent quarks. In general, they predict P_V to be less than 0.75.

The situation is complicated by the presence of mesons with non-zero orbital angular momentum. The observed P_V ratio thus includes those ground state mesons which have been produced in decays of the excited states. Experimentally, this effective ratio $P_V^{\rm eff}$ is easier to measure. If the production rates of the excited states are known, the primary ratio $P_V^{\rm prim}$, corrected for any effects from excited states, can be calculated. The LEP accelerator, where numerous $Z^0 \to q\bar{q}$ decays have been observed between 1989 and 1995, provides a facility to study the P_V ratio. Values around $P_V^{\rm eff} \approx 0.75$ and $P_V^{\rm eff} \approx 0.55$ have been measured for B meson production [2] and in the charm sector [3,4], respectively. In both cases, a model dependent evaluation suggests the values of $P_V^{\rm prim}$ and $P_V^{\rm eff}$ to be similar [5]. For light mesons, $P_V^{\rm eff}$ has been estimated to be between 0.4 and 0.5 [6]. This paper focuses on a study of both $P_V^{\rm eff}$ and $P_V^{\rm prim}$ for charmed meson production.

In the charm system, measurements of D^0, D^+, and D^{*+} production in $Z^0 \to c\bar{c}$ decays have been used in the previous determinations of $P_V^{\rm eff}$ [3,4]. The D^{*0} meson has so far not been observed in Z^0 decays, since it only decays via the emission of a photon or a π^0 meson, which are difficult to reconstruct experimentally. Therefore, the determinations of P_V values have so far relied on the assumption of isospin invariance, which suggests equal D^{*0} and D^{*+} production rates.

In this paper, a first measurement of the hadronisation fraction $f(c \to D^{*0})$ in $Z^0 \to c\bar{c}$ decays is presented. The analysis is based on more than 4 million hadronic Z^0 decays recorded with the OPAL detector at the LEP accelerator in the years 1990 to 1995. The D^{*0} mesons are reconstructed in the decay channels $D^{*0} \to D^0\gamma$ and $D^{*0} \to D^0\pi^0$. The same techniques are applied in the $D_s^+\gamma$ final state for the reconstruction of D_s^{*+} mesons, which at LEP have only been observed in leptonic D_s^+ decays [7]. The $f(c \to D^{*0})$ measurement is used to test the assumption of isospin invariance. Together with previously published OPAL measurements of the other charmed non-strange pseudoscalar and vector mesons [8,9], a value of $P_V^{\rm eff}$ is derived. A recent OPAL measurement of the production of excited charmed mesons [10] is used to investigate the ratio $P_V^{\rm prim}$. A model independent formula for $P_V^{\rm prim}$ is derived, and the validity of a simple spin counting model for the fragmentation process is tested.

[1] "Spin counting" in this paper refers to a model where the relative primary production of mesons with the same quark content and the same orbital angular momentum is given according to the corresponding numbers of spin degrees of freedom.

The paper is organized as follows: Sect. 2 contains a brief description of the OPAL detector and the event selection. Section 3 describes the reconstruction of D^{*0} decays, the selection of signal candidates, and the background determination. In Sect. 4, the measurement of the hadronisation fraction $f(c \to D^{*0})$ and its systematic uncertainties are discussed, while Sect. 5 describes the measurement of D_s^{*+} production. Section 6 contains a determination of both $P_V^{\rm eff}$ and $P_V^{\rm prim}$ for charmed meson production in $Z^0 \to c\bar{c}$ decays and an interpretation of the results.

2 The OPAL detector and event selection

A complete description of the OPAL detector is given elsewhere [11]. Here, only the components of importance for this analysis are reviewed. Tracking of charged particles is performed by a silicon microvertex detector, a vertex detector, a jet chamber, and a set of drift chambers that measure the coordinate of tracks along the direction of the beam line[2] (z-chambers), positioned inside a solenoid that provides a uniform magnetic field of 0.435 T parallel to the beam direction.

The barrel electromagnetic calorimeter, which covers the polar angle range of $|\cos\theta| < 0.82$, is mounted outside the magnet coil. It consists of a cylindrical array of 9,440 lead glass blocks of 24.6 radiation lengths thickness pointing approximately to the interaction region. The overall energy resolution is improved by correcting for the energy lost in showers initiated in the material in front of the calorimeter. Such showers are detected by thin gas detectors (presampler detectors) situated in front of the lead glass blocks, and by time-of-flight scintillators located between the presampler and the magnet coil in the polar angle range $|\cos\theta| < 0.72$. The regions $0.82 < |\cos\theta| < 0.98$ are covered by the endcap electromagnetic calorimeters with lead glass blocks oriented parallel to the beam direction. The magnet return yoke is instrumented as a hadron calorimeter. Four layers of muon chambers are mounted outside the hadron calorimeter.

The criteria for selecting hadronic Z^0 decays are based on reconstructed tracks in the central detector and on the energy distribution in the calorimeter [12]. Charged particle tracks need to have at least 20 jet chamber hits, a momentum component in the xy plane of at least 0.15 GeV, a total momentum of less than 65 GeV, and a distance of closest approach to the beam axis of less than 5 cm. The hadronic Z^0 event selection efficiency of these requirements is $(98.7 \pm 0.4)\%$ [9]. Of the events recorded with the OPAL detector between 1990 and 1995, 4.32 million satisfy the event selection criteria. The primary vertex is reconstructed from the charged tracks in the event and constrained with the known average beam position and the xy width of the e^+e^- collision point.

[2] The OPAL coordinate system is defined with positive z along the electron beam direction and the x axis horizontal; θ and ϕ are the polar and azimuthal angles, respectively.

Samples of simulated hadronic events are used for the determination of selection criteria and for the calculation of selection efficiencies. They have been generated using the JETSET 7.4 Monte Carlo model [13] with parameters tuned to reproduce the OPAL data [14]. The fragmentation of heavy quarks is parametrised by the fragmentation function of Peterson et al. [15]. The simulated events are then processed by the detector simulation program [16] and by the same reconstruction algorithm which is also applied to the data.

3 Reconstruction and selection of D^{*0} candidates

In Z^0 decays, D^{*0} mesons are dominantly produced in $Z^0 \to c\bar{c}$ events and in the decay of bottom hadrons. The D^{*0} mesons are reconstructed in the decay modes $D^{*0} \to D^0\gamma$ and $D^{*0} \to D^0\pi^0$. The transition photon or π^0 meson is expected to be dominantly produced in the core of the jet that contains the D^{*0}. Thus, for the reconstruction of $D^{*0} \to D^0\gamma$ decays, a considerable background level is expected from photons originating in decays of π^0 mesons from other sources, while the reconstruction of $D^{*0} \to D^0\pi^0$ decays suffers from combinatorial background in the $\pi^0 \to \gamma\gamma$ reconstruction. The reconstruction proceeds by first finding D^0 candidates, which are then combined with a photon or a π^0. After a loose preselection, a likelihood method is used for the final selection of candidates. In this section, the selection and the background determination are described.

3.1 Reconstruction of D^0 mesons, photons, and π^0 mesons

Both the preselection for the D^0, photon, and π^0 reconstruction and the likelihood for the D^{*0} selection are based on the variables which are explained below.

The decay mode $D^0 \to K^-\pi^+$ is used to reconstruct D^0 mesons. Initially, all possible pairs of oppositely charged tracks are formed, assigning kaon and pion masses to the tracks. Variables for the selection of D^0 candidates are:

- the invariant mass m_{D^0} and the scaled energy $x_{D^0} = E_{D^0}/E_{\mathrm{beam}}$ of the D^0 candidate;
- the cosine of the helicity angle θ^* measured between the direction of the charged pion in the D^0 rest frame and the D^0 direction in the laboratory frame;
- the signed probability W_X as defined in [17] that a given track is compatible with the particle hypothesis X, based on its specific energy loss and its measured momentum;
- the signed decay length d_{xy} in the xy plane defined as the distance between the primary vertex and the secondary vertex formed by the D^0 decay products; and
- the largest longitudinal momentum p^l_{frag} relative to the D^0 flight direction of any track which is not used in the D^0 reconstruction and whose charge is inconsistent with that of an accompanying hadron of the D^0 candidate. This variable helps to separate signal candidates in $Z^0 \to c\bar{c}$ events from background, since in the formation of D^0 mesons in $Z^0 \to c\bar{c}$ events, there is a correlation between the charge of the primary quark and that of the fragmentation particle with the highest longitudinal momentum [18]. The track with the largest longitudinal momentum whose charge is inconsistent with being the accompanying hadron is expected to be softer for signal than for background.

Table 1. The preselection cuts for the reconstruction of D^{*0} candidates. The selection variables are defined in the text

D^0 reconstruction
$1.81\,\mathrm{GeV} < m_{D^0} < 1.93\,\mathrm{GeV}$
$0.3 < x_{D^0}$
$-0.85 < \cos\theta^* < 0.85$
$W_K(K) < -1\%$ or $+3\% < W_K(K)$
$-35\% < W_\pi(K) < 0\%$
$W_\pi(\pi) < -1\%$ or $+1\% < W_\pi(\pi)$
photon and π^0 reconstruction
$800\ \mathrm{MeV} < E_\gamma$ or $800\ \mathrm{MeV} < E_{\pi^0}$
$60\ \mathrm{MeV} < m_{\gamma\gamma} < 280\ \mathrm{MeV}$

Contributions from D^{*+} decays are suppressed by searching for a track that could have been the pion in a $D^{*+} \to D^0\pi^+$ decay. The corresponding D^0 candidate is rejected if a track is found with the correct charge and a mass difference within $141\ \mathrm{MeV} < m_{D^0\pi^+} - m_{D^0} < 152\ \mathrm{MeV}$.

A loose preselection of D^0 candidates is done using the invariant mass m_{D^0}, the scaled energy x_{D^0}, the helicity angle $\cos\theta^*$, and the particle identification probabilities. The exact cuts are listed in Table 1.

Photons are reconstructed either as showers in the electromagnetic calorimeter, or through conversions $\gamma \to e^+e^-$. For the latter, pairs of oppositely charged tracks are identified as conversions with the algorithm described in [19]. The z components of the track momenta are determined in a fit to the conversion point to improve the momentum resolution. The total photon momentum is taken as the sum of both track momenta.

In the barrel region of the electromagnetic calorimeter, photons are identified as described in [19] by fitting electromagnetic showers to energy deposits which are not associated with any charged particle track. The lateral shower profile is fixed to the Monte Carlo expectation, and the normalisation gives the shower energy. The fitted shower energy is then corrected for losses in the material in front of the calorimeter using information from the presampler and time-of-flight system. Each of the fitted showers is treated as a photon candidate. The photon momenta are calculated assuming that the photons originated at the primary vertex of the event.

Any pair of photons (showers or conversions) with an invariant mass between 60 MeV and 280 MeV is considered as a π^0 candidate. The resolution of the π^0 energy

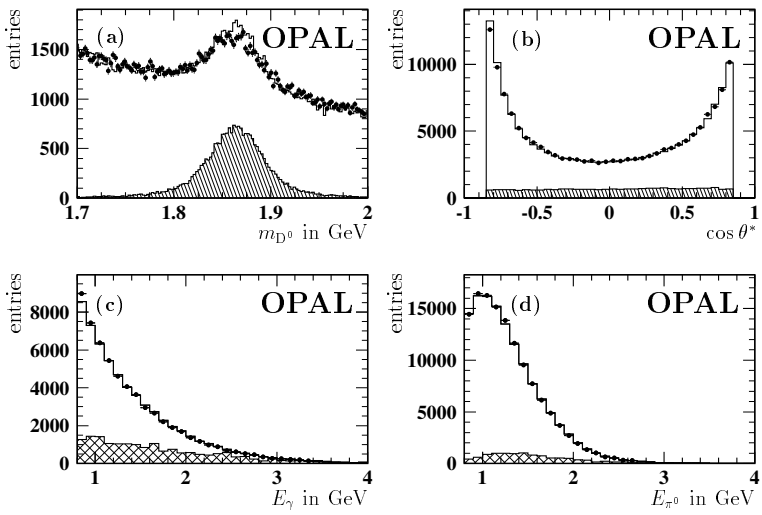

Fig. 1a–d. The distributions of the four D^{*0} selection variables m_{D^0}, $\cos\theta^*$, E_γ and E_{π^0} are shown for all preselected candidates. In each case, points with error bars correspond to the data and the open histogram to the simulation, scaled to the same number of entries. In **a**, **b**, the contribution from D^{*0} candidates with a correctly reconstructed $D^0 \to K^-\pi^+$ decay is shown as the hatched area. The cross-hatched areas in **c** and **d** correspond to 10 times the contribution of correctly reconstructed photons or π^0 mesons from a D^{*0} decay

is improved by a constraint to the nominal π^0 mass [20] using a kinematic fit [19].

A number of variables similar to those in reference [19] are calculated for each photon and π^0 candidate:

- the energy of the photon or π^0 candidate, denoted E_γ or E_{π^0}, respectively;
- for photon conversions, the signed electron identification probabilities W_e calculated from the energy loss of the two conversion tracks;
- for showers in the calorimeter, a variable which parametrises how well the fitted shower describes the measured energy distribution in the 9 calorimeter blocks around the fitted shower maximum; and three variables that describe their effective separation from the closest neighbouring shower and the closest charged track entering the calorimeter.

The following variables are only used in the selection of π^0 mesons:

- the invariant mass of the $\gamma\gamma$ system and the opening angle between the two photons; as well as
- the number of additional photon candidates in a cone around each of the two photon candidates under consideration. In each case, the opening angle of the cone is twice the angle between the two photons.

A loose preselection of photons and π^0 candidates is done using the photon or π^0 energy and the invariant $\gamma\gamma$ mass before the constraint to the π^0 mass, as listed in Table 1.

To form D^{*0} candidates, each of the preselected D^0 candidates is in turn combined with every preselected shower photon or π^0 candidate in the event. Fig. 1a–d shows the distribution of these D^{*0} candidates in four of the most powerful selection variables. Tighter requirements are then applied to further reduce the background level in the D^{*0} sample. They are based on the variables listed above and on the total number of D^{*0} candidates in the hemisphere. For each variable x_i, a purity function $\lambda_i(x_i)$ is calculated based on the simulation as the ratio of $c \to D^{*0}$ signal candidates to all candidates:

$$\lambda_i(x_i) = \frac{signal}{(signal + background)}(x_i)\,, \qquad (1)$$

and a likelihood is constructed as

$$\mathcal{L}(x_1, ..., x_n) = \left(\prod_{i=1}^{n} \lambda_i(x_i)\right)^{1/n}. \qquad (2)$$

Finally, D^{*0} candidates are selected using a cut on the likelihood value. This cut has been chosen such that the statistical error on the result for the hadronisation fraction $f(c \to D^{*0})$ is minimised according to an independent sample of simulated events. The distributions of the likelihood functions $\mathcal{L}$ are shown in Fig. 2a,b together with the cut values.

In Fig. 3a–h, the $\Delta m = m_{D^{*0}} - m_{D^0}$ mass difference distributions of the selected candidates are shown. The peaks at low mass differences are due to the signal from D^{*0} decays. The background shape is determined from the data as described below in Sect. 3.2. Using this shape, the D^{*0} yield is extracted from a fit to the mass difference distributions, which is discussed in Sect. 4.2.

3.2 Background determination

Even after applying the likelihood selection, the background level in the samples of D^{*0} candidates is still high. To minimise the dependence on Monte Carlo modelling, a method has been developed to determine the shape of the background in the Δm distributions from the data.

A sample of candidates enriched in background rather than signal is prepared with a method similar to the one for the signal selection (see Sect. 3.1). The likelihood is modified to select background candidates from the m_{D^0} sideband regions 1.70 GeV $< m_{D^0} <$ 1.84 GeV and 1.91 GeV $< m_{D^0} <$ 2.00 GeV. The sidebands are chosen to lie close to the signal region so that the kinematical properties of candidates in the sidebands do not differ significantly from those of candidates in the signal region.

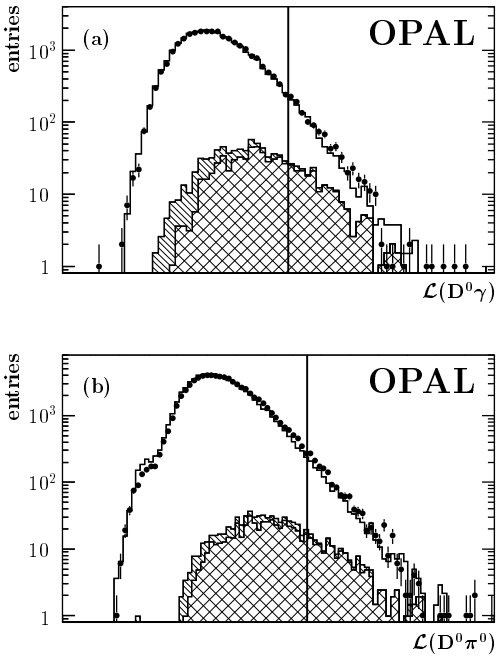

Fig. 2a,b. The distributions of the likelihood functions $\mathcal{L}$ for the two D^{*0} decay channels. Points with error bars represent the data and open histograms the simulation, scaled to the same number of entries. The hatched histograms show candidates in the simulation with a correctly identified photon or π^0 from a D^{*0} decay; for candidates entering the cross-hatched histogram, the $D^0 \to K^-\pi^+$ decay is also correctly reconstructed. The vertical lines represent the cuts on the likelihood functions. No scale is given for the likelihood values since only the relative position of the cut is relevant

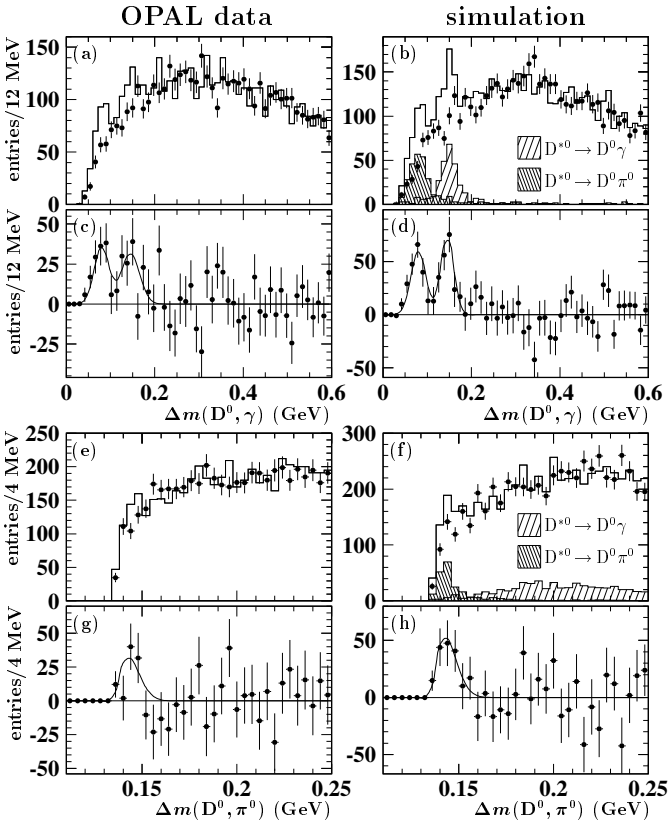

Fig. 3a–h. The $\Delta m(D^0,\gamma)$ and $\Delta m(D^0,\pi^0)$ mass difference distributions in the data and the simulation.
In **a**, **b**, **e**, and **f**, the distributions obtained in the signal selection procedure are shown as solid histograms, and those obtained in the background selection procedure as points with error bars, where the relative normalisation of the latter distribution has been determined in the fit. In addition, the hatched histograms show the distributions of signal candidates reconstructed in the simulation with the signal selection procedure. In **c**, **d**, **g**, and **h**, the corresponding background subtracted distributions are shown together with the fit results; the error bars show the statistical errors only

The modified likelihood function is of the form

$$\mathcal{L}'(x_1,...,x_n) = \left(\lambda'_{m_{D^0}}(m_{D^0})\,\lambda'_{\cos\theta^*}(\cos\theta^*)\prod_{x_i\neq m_{D^0},\cos\theta^*}\lambda_i(x_i)\right)^{1/n}, \quad (3)$$

with the λ functions left unchanged for all selection variables except m_{D^0} and $\cos\theta^*$. Because the original likelihood function $\mathcal{L}$ depends on m_{D^0} and $\cos\theta^*$, new functions $\lambda'_{m_{D^0}}(m_{D^0})$ and $\lambda'_{\cos\theta^*}(\cos\theta^*)$ have to be introduced such that the shapes of the distributions of the likelihoods $\mathcal{L}$ and $\mathcal{L}'$ agree for background. In practise, this is done by constructing the λ' functions for m_{D^0} and $\cos\theta^*$ separately, with the same set of values as for the corresponding λ function. For the selection of background candidates, the same cut is placed on $\mathcal{L}'$ as is on $\mathcal{L}$ for signal candidates.

One of the main requirements for the background selection is that it correctly reproduces the Δm shape of true background. If the selection variables m_{D^0} and $\cos\theta^*$ are assumed to be uncorrelated with the other selection variables and the mass difference Δm, the Δm shapes of background candidates from the same source in the signal and background samples agree by construction. For true background, the correlations between m_{D^0} ($\cos\theta^*$) and any other selection variable have been found in the simulation to be $\leq 1\%$ ($< 10\%$), where the largest correlations are between $\cos\theta^*$ and $p^l_{\rm frag}$ (-9%) or $W_\pi(\pi)$ (-7%). It has been tested in the simulation that even with this level of correlations, the background shape is correctly reproduced for background candidates from the same source.

Background can be classified into candidates where a correctly reconstructed D^0 is combined with a photon or π^0 that does not come from a D^{*0} decay and other background, in which the charged pion and kaon candidates do not come from the same D^0 decay. For these two contributions, the shapes of the Δm distributions are found to be slightly different in the simulation. As outlined above, it is expected that the background determination procedure yields the correct background shapes individually for both contributions. However, the background sample contains fewer candidates with a correctly reconstructed D^0

than the signal sample. This leads to a small bias in the overall background shape derived from the background selection, which is taken into account by reweighting this shape according to the sample composition in the signal and background samples as found in the simulation.

Candidates that pass the cuts on $\mathcal{L}$ and also on $\mathcal{L}'$ are rejected from both the signal and the background samples. In the simulation, it has been found that this requirement rejects 8% of the true signal from the signal sample, and 27% of the true signal in the background sample. It has also been verified that the fraction of candidates removed by this requirement is the same within errors for the data and the simulation.

Although the background sample is depleted in signal candidates relative to the signal sample, there is a remaining D^{*0} signal contamination in the background sample. Typically, the signal fraction is a factor of 5 smaller (cf. Table 2) in the background samples. These candidates have the effect of reducing the number of signal candidates after background subtraction and are taken into account by calculating an effective efficiency, which is described in the next section.

3.3 Reconstruction efficiency

The efficiencies of the D^{*0} reconstruction are determined from a Monte Carlo sample which is statistically independent from the one that has been used for the determination of the likelihood. In this sample of 6.5 million simulated hadronic events, the numbers of true D^{*0} mesons that pass the cuts on $\mathcal{L}$ are computed. The resulting efficiencies in the different decay modes are listed in Table 2, separately for $Z^0 \to c\bar{c}$ and $Z^0 \to b\bar{b}$ events.

As discussed in Sect. 3.2, some D^{*0} mesons are also contained in the background-enriched samples. This number is determined from the same set of simulated events, and an effective efficiency is computed from the values given in Table 2 that takes into account the relative signal to background ratio of the background sample that is given in the last column of the table. In the fit to the mass difference distributions described in Sect. 4.2, these effective efficiencies are used.

4 Measurement of $f(c \to D^{*0})$

The dominant sources of D^{*0} mesons in Z^0 decays are the production in $Z^0 \to c\bar{c}$ events and in bottom hadron decays. For scaled energies $x_{D^0} > 0.3$, the production of D^{*0} mesons in gluon splitting processes $g \to c\bar{c}$ is highly suppressed and will be neglected in the following.

The hadronisation fraction $f(c \to D^{*0})$ is determined in a fit to the $\Delta m = m_{D^{*0}} - m_{D^0}$ distributions of the selected signal and background samples. A simultaneous fit is performed to the Δm distributions of both $D^0\gamma$ and $D^0\pi^0$ candidates. In the fit, the contributions from b hadron decays are subtracted, and the fitted signals are corrected for the efficiency in $Z^0 \to c\bar{c}$ events. In this section, the determination of the signal contributions from b hadron decays, the fit to the mass difference distributions, and systematic uncertainties of the measurement are discussed.

4.1 Subtraction of the component from b hadron decays

The determination of the contribution from b hadron decays is based on a previous measurement of D^{*+} production in $Z^0 \to b\bar{b}$ events [9]. This measurement is used to assess the corresponding D^{*0} production rate under the assumption that the CLEO measurement [21] of

$$\frac{Br(B \to D^{*0} X)}{Br(B \to D^{*+} X)} = 1.03 \pm 0.14 \qquad (4)$$

can be transferred to LEP energies. The subtraction of the component from $Z^0 \to b\bar{b}$ events is done for scaled energies $x_{D^0} > 0.3$, and the remaining $c \to D^{*0}$ signal is then extrapolated to the full x_{D^0} range. The error on the CLEO measurement is taken into account as described in Sect. 4.4.4. Decays of $\overline{B}^0$ and B^- mesons account for most D^{*0} mesons from b hadron decays at LEP, since $\overline{B}^0_s$ mesons preferentially decay to final states with a D_s^+ [20], and b baryons are expected to decay dominantly to final states with a c baryon.

Previously, OPAL has measured the production of D^{*+} mesons in $Z^0 \to b\bar{b}$ events to be $R_b\, f(b \to D^{*+})\, Br(D^{*+} \to D^0\pi^+)\, Br(D^0 \to K^-\pi^+) = (1.334 \pm 0.049 \pm 0.078) \times 10^{-3}$ [9], where R_b is the partial hadronic decay width of the Z^0 boson into $b\bar{b}$ pairs. Using this number and the branching fraction $Br(D^{*+} \to D^0\pi^+) = 0.683 \pm 0.014$ [20], the D^{*+} production rate in $Z^0 \to b\bar{b}$ events for $x_{D^0} > 0.3$ is calculated to be

$$\beta \equiv R_b\, f(b \to D^{*+})\, Br(D^0 \to K^-\pi^+)\big|_{x_{D^0}>0.3} = (0.980 \pm 0.068) \times 10^{-3}\ . \qquad (5)$$

The error includes both the statistical and systematic errors. The restriction to $x_{D^0} > 0.3$ is based on Monte Carlo simulation and the measured parameters of the b fragmentation function.

This information is used to obtain the number of reconstructed D^{*0} signal candidates from b hadron decays, which is then subtracted from the fitted signal. Thus, the hadronisation fraction $f(c \to D^{*0})\big|_{x_{D^0}>0.3}$ is determined in the fit from

$$R_c\, f(c \to D^{*0})\, Br(D^0 \to K^-\pi^+)\big|_{x_{D^0}>0.3} = \qquad (6)$$

$$\sum_{X=\gamma,\pi^0} \frac{\frac{N_{sig}(D^{*0} \to D^0 X)}{2N_{had}} - \beta\, Br(D^{*0} \to D^0 X)\, \varepsilon_b^{D^{*0} \to D^0 X}}{\varepsilon_c^{D^{*0} \to D^0 X}},$$

where R_c is defined in analogy to R_b, N_{sig} denotes the signal as obtained from the mass difference distribution, N_{had} is the number of hadronic Z^0 decays analysed, ε_c and ε_b are the effective efficiencies for reconstructing D^{*0} decays with $x_{D^0} > 0.3$ from $Z^0 \to c\bar{c}$ and $Z^0 \to b\bar{b}$ decays,

Table 2. The reconstruction efficiencies for a given decay chain in a given mass difference distribution as determined from the simulation. Note that $D^{*0} \to D^0\pi^0$ decays are measured in both the $\Delta m(D^0,\gamma)$ and $\Delta m(D^0,\pi^0)$ distributions. The efficiencies are based on candidates with scaled energies $x_{D^0} > 0.3$. Only statistical errors are listed. The signal to background ratios $(\frac{s}{b})^{bkg}$ in the background samples relative to the ratio $(\frac{s}{b})^{sig}$ in the corresponding signal sample are given in the last column

decay chain	distribution	efficiency, $c \to D^*$	efficiency, $b \to D^*$	$(\frac{s}{b})^{bkg}/(\frac{s}{b})^{sig}$
$D^{*0} \to D^0\gamma$				
$\hookrightarrow K^-\pi^+$	$\Delta m(D^0,\gamma)$	$(2.88 \pm 0.16)\%$	$(2.15 \pm 0.19)\%$	0.20 ± 0.03
$D^{*0} \to D^0\pi^0$	$\Delta m(D^0,\gamma)$	$(1.80 \pm 0.10)\%$	$(1.01 \pm 0.10)\%$	0.20 ± 0.03
$\hookrightarrow K^-\pi^+$	$\Delta m(D^0,\pi^0)$	$(1.18 \pm 0.08)\%$	$(1.05 \pm 0.10)\%$	0.16 ± 0.01

respectively, and the sum runs over the two decay modes of the D^{*0}.

4.2 The fit to the mass difference distributions

The number of reconstructed D^{*0} decays is determined in a simultaneous fit to the mass difference distributions of the selected signal and background samples in the two decay modes $D^{*0} \to D^0\gamma$ and $D^{*0} \to D^0\pi^0$.

Two signal peaks are visible in the mass difference distribution of $D^0\gamma$ candidates, which is shown in Fig. 3. The peak at the nominal D^{*0}–D^0 mass difference of 142 MeV [20] is due to $D^{*0} \to D^0\gamma$ decays, whereas the one at lower Δm values is from $D^{*0} \to D^0\pi^0$ decays, where only one photon from the π^0 decay is combined with the D^0 candidate.

In the mass difference distribution of $D^0\pi^0$ candidates, the signal from $D^{*0} \to D^0\pi^0$ decays is expected around the nominal mass difference. Additional contributions are expected from $D^{*0} \to D^0\gamma$ and $D^{*0} \to D^0\pi^0$ decays, where only one of the two photons from the π^0 decay is used. In both cases, an unrelated photon candidate is added to form a π^0 candidate. In the simulation, both contributions have been found to be broad and very similar in shape to the overall background. Therefore, they are not explicitly accounted for.

In both mass distributions, the signal is parametrised with a functional form, while the background shape is determined from the background sample as decribed in Sect. 3.2, with its normalisation determined in the fit. A sum of two Gaussians is used as signal parametrisation for the Δm distribution of $D^0\gamma$ candidates (see Figs. 3c and d) in order to accommodate the contributions from both $D^{*0} \to D^0\gamma$ and $D^{*0} \to D^0\pi^0$ decays. The mean values of the Gaussians are fixed to 145 MeV ($D^{*0} \to D^0\gamma$) and 80 MeV ($D^{*0} \to D^0\pi^0$) as determined from the simulation, and the widths are allowed to vary. For $D^0\pi^0$ candidates, a modified Gaussian of the form

$$\frac{\mathrm{d}n}{\mathrm{d}(\Delta m)} \sim (\Delta m - m_{\pi^0}) \ \exp\left(-\frac{1}{2}\left(\frac{\Delta m - m_{\pi^0}}{\sigma}\right)^2\right); \quad \Delta m > m_{\pi^0} \tag{7}$$

is taken as the signal parametrisation (see Fig. 3g and h) to account for threshold effects. Here, m_{π^0} denotes the nominal π^0 mass [20], and the parameter σ and the normalisation are determined in the fit. In the simulation, such a function has been found to parametrise the distribution of $D^0\pi^0$ signal candidates well.

The hadronisation fraction $f(c \to D^{*0})$ is determined from a simultaneous fit to both Δm distributions, with the constraint that the efficiency corrected number of $D^{*0} \to D^0\pi^0$ decays be the same whether determined from the peak at lower Δm values in the $\Delta m(D^0,\gamma)$ distribution or from the $\Delta m(D^0,\pi^0)$ distribution. Also, the efficiency corrected numbers for the two D^{*0} decay channels are fixed to the world average value of the branching ratio $Br(D^{*0} \to D^0\gamma)/Br(D^{*0} \to D^0\pi^0) = 0.616 \pm 0.076$ [20], and it is assumed that these two decay modes saturate the D^{*0} width. The contribution from bottom hadron decays, which is derived from an earlier OPAL measurement as described in Sect. 4.1, is subtracted in the fit.

The fit results are illustrated in Fig. 3, where the obtained signal parametrisations are shown together with the background subtracted mass difference distributions. The combined fit for the D^{*0} measurement has a χ^2 of 61.6 for 69 degrees of freedom. The hadronisation fraction $f(c \to D^{*0})\big|_{x_{D^0}>0.3}$ is extrapolated to the full range of scaled energies x_{D^0} using the simulation; it is found to be

$$R_c\, f(c \to D^{*0})\, Br(D^0 \to K^-\pi^+) = (1.44 \pm 0.36) \times 10^{-3}, \tag{8}$$

where the error is statistical.

4.3 Consistency checks

A number of consistency checks has been performed, in particular to test the sensitivity of the result to the background subtraction procedure. Monte Carlo simulation has been used to check that the procedure as outlined in Sect. 3.2 accurately describes the shape of the background in the signal sample. Also, it has been verified that the shape is not sensitive to the specific choice of λ' functions. The background determination is sensitive to correlations between m_{D^0} or $\cos\theta^*$ and any other selection variable. Any correlation seen in the data is well reproduced in the simulation. Finally, the analysis has been repeated on the simulation, and the generated rates are reproduced within the statistical errors.

Table 3. A breakdown of the relative statistical and systematic errors on the hadronisation fraction $f(c \to D^{*0})$

relative statistical error	24.9%
relative systematic errors:	
modelling of selection variables:	
D^0 mass resolution	1.3%
$\langle x(D^*)\rangle_{Z^0 \to c\bar{c} \to D^{*0}}$	3.9%
$\langle x(X_b)\rangle_{Z^0 \to b\bar{b} \to X_b}$	3.0%
D^0 lifetime	0.8%
D^{*0} spin alignment	0.3%
effective shower isolation	9.7%
photon pair opening angle	2.8%
number of π^0 candidates	0.2%
number of D^{*0} candidates	1.3%
dE/dx	3.6%
dE/dx preselection cuts	3.1%
fragmentation tracks	2.7%
shower fit	5.9%
detector resolution:	
tracking resolution	6.4%
calorimeter energy scale and resolution	1.7%
fit procedure:	
background normalisation	3.4%
$Br(D^{*0} \to D^0\gamma)/Br(D^{*0} \to D^0\pi^0)$	2.0%
background shape	5.5%
contributions from other D^0 decays	0.4%
contributions from D^{*+} and D_s^{*+} decays	1.4%
b subtraction and extrapolation:	
subtraction of the $b \to D^{*0}$ contribution	12.2%
extrapolation to $x_{D^0} = 0$	1.2%
total relative systematic error	20.9%

For all selections, the likelihood cut has been varied and the analysis repeated. The ranges of cut values correspond to relative changes in efficiency of about ±50%. The variations have been found to be consistent with statistical fluctuations.

In the fit, the ratio $Br(D^{*0} \to D^0\gamma)/Br(D^{*0} \to D^0\pi^0)$ is fixed to its world average value of 0.616 ± 0.076 [20]. If instead, it is allowed to vary, a value of $Br(D^{*0} \to D^0\gamma)/Br(D^{*0} \to D^0\pi^0) = 0.39 \pm 0.17\,(stat.)$ is found, which is consistent with the world average. The resulting hadronisation fraction $f(c \to D^{*0})$ changes by -7.5%.

4.4 Systematic uncertainties

Systematic uncertainties are related to the modelling of the selection variables, the detector resolution, the procedure used to subtract the background, the determination of the $b \to D^{*0}$ contribution to the measured signal, and to the extrapolation to the full range of scaled energies x_{D^0}. In the following sections, each of these categories is discussed in turn. The relative values of all errors are listed in Table 3.

4.4.1 Uncertainties from the modelling of selection variables

Possible differences between distributions in data and simulation could influence the efficiencies and the background determination. These effects are studied separately for each selection variable. The resulting systematic errors are assumed to be uncorrelated and are therefore added in quadrature.

Two principal methods are used to determine systematic uncertainties in the modelling of a selection variable: **(A)** Variables for which the distributions of signal candidates are measured are treated by reweighting the events in the Monte Carlo simulation such that for the weighted events, the simulated signal distribution agrees with the measured one. Using the likelihood given in equation (2), the background determination and the fit are then repeated and the original result is corrected according to the observed difference; the uncertainty in the difference is interpreted as a systematic error. This method takes correlations between the selection variables into account to the extent that in the case of non-zero correlations, the reweighting of events alters also the distribution of any variable that is correlated with the one variable in question. This procedure is applied

- to the invariant mass distribution of D^0 candidates,
- to the Peterson et al. fragmentation parameters which have been varied in the ranges corresponding to mean scaled energies of D^{*0} mesons in $Z^0 \to c\bar{c}$ decays of $0.506 < \langle x(D^{*0})\rangle_{Z^0 \to c\bar{c} \to D^*} < 0.531$ and of weakly decaying b hadrons in $Z^0 \to b\bar{b}$ decays of $0.702 < \langle x(X_b)\rangle_{Z^0 \to b\bar{b} \to X_b} < 0.730$ [22], respectively[3],
- to the lifetime of D^0 mesons, which has been varied within $\tau_{D^0} = (0.415 \pm 0.004)$ ps [20],
- to the distributions of energies E_γ and E_{π^0}, where the simulated events are reweighted such that the helicity angle distributions in $D^{*0} \to D^0\gamma$ and $D^{*0} \to D^0\pi^0$ decays agree with the measured D^{*+} spin alignment in $Z^0 \to c\bar{c}$ events (the spin density matrix element is $\rho_{00} = 0.40 \pm 0.02$ [23]),
- to the effective separation of a shower from the closest other shower in the electromagnetic calorimeter,
- to the opening angle of a pair of photons, and
- to the numbers of reconstructed π^0 and D^{*0} candidates.

The last three of the above variables depend on the event topology. For these variables, possible deviations between data and simulation affect the signal and the background in the same way. The simulated events are therefore reweighted such that the distributions of all candidates in data and simulation agree. The analysis is then repeated, and the observed difference in the fit result is treated as a systematic error.

(B) The second method is used for the remaining selection variables, which are

[3] These variations in the mean energies are larger than the current errors and account also for errors related to the modelling of the shapes of the fragmentation functions.

- the track probabilities calculated from dE/dx information,
- the largest longitudinal momentum of fragmentation tracks inconsistent with being an accompanying hadron, and
- the goodness of the shower fit.

The corresponding function $\lambda_i(x_i)$ is set to its maximum value for one variable x_i at a time. The resulting modified likelihood functions $\mathcal{L}_i$ and $\mathcal{L}'_i$ are independent of that particular variable x_i, so using these functions instead of the original likelihoods removes any possible bias due to the simulation of x_i. The selection of the signal and background D^{*0} candidate samples is repeated with these modified likelihoods. By construction, these samples also contain those candidates selected with the original likelihoods $\mathcal{L}$ and $\mathcal{L}'$. The ratio of the fit results obtained with the original $(\mathcal{L}, \mathcal{L}')$ and the modified $(\mathcal{L}_i, \mathcal{L}'_i)$ likelihoods is calculated for the data and the simulation, where the statistical correlation between the samples is taken into account. The relative difference of these ratios is interpreted as the systematic error associated with the variable x_i. In the case of the signed particle identification probabilities, the cuts for the preselection of charged kaons and pions (see Sect. 3.1) are retained in order to obtain a clear signal. In [8], an error of 3.1% has been determined for these cuts in the D^0 selection. This error is included as an additional systematic uncertainty.

4.4.2 Uncertainties in the detector resolution

Tracking resolution:
Uncertainties in the modelling of the central detector are assessed by repeating the analysis with the tracking resolutions varied by ±10% around the values that describe the data best. The redetermined efficiencies are compared with the original ones, and the relative difference is interpreted as a systematic error.

Calorimeter energy scale and resolution:
The energy scale and resolution of the electromagnetic calorimeter and the multiplicity and resolution in the time-of-flight scintillators are treated analogously. The reconstructed π^0 mass distribution has been used to determine the corresponding resolution and scaling parameters. Thus, width and position of the π^0 mass peak are well reproduced in the simulation [19], and any possible bias is accommodated by the variation of the detector resolution.

4.4.3 Uncertainties in the fit procedure

Background normalisation:
To check the determination of the background normalisation, the fit to the mass difference distributions has been repeated with the range restricted to values of $\Delta m(D^0, \gamma)$<0.4 GeV and $\Delta m(D^0, \pi^0)$<0.2 GeV. Deviations from the previous results were interpreted as systematic errors.

D^{*0} branching ratio:
The fit to the $\Delta m(D^0, \gamma)$ and $\Delta m(D^0, \pi^0)$ distributions is constrained to the world average of the branching ratio $Br(D^{*0} \to D^0\gamma)/Br(D^{*0} \to D^0\pi^0) = 0.616 \pm 0.076$ [20]. The fit is repeated with this ratio varied within its errors, and the observed difference is taken as a systematic error.

Background shape:
Background candidates with a correctly reconstructed D^0 lead to a bias in the Δm distribution, which is taken into account in the background subtraction as outlined in Sect. 3.2. The analysis has been repeated without correcting for this bias, and half the difference from the original result is assigned as a systematic error.

The origin of background candidates has been studied in the simulation, and no other source for a bias of the background shape has been identified. In particular, it has been checked that the contribution from photons or π^0 mesons from D^{**}, B^*, and B^{**} decays is small and does not exhibit a pronounced structure.

Contributions from other D^0 decays:
In the simulation, the contribution to the signal sample of D^{*0} candidates from D^0 mesons not decaying to $K^-\pi^+$ was found to be 5.9%. This contribution is accounted for in the efficiency determination. However, mismodelling of the branching fractions for these other decay modes can introduce a potential bias in the D^{*0} measurement. The corresponding systematic error is evaluated assuming relative contributions of other decay modes as in [9] and assigning errors according to the errors on the branching fractions as given in [20].

Contributions from D^{*+} and D_s^{*+} decays:
In the reconstruction of D^{*0} decays, there are contributions from D^{*+} and D_s^{*+} mesons, which can also decay via γ or π^0 emission. In principle, these decays can lead to a signal in the Δm distributions similar to that to be measured. However, it has been found in the simulation that the relative contribution from D^{*+} and D_s^{*+} decays to the selected signal and background samples is approximately equal. A small correction is applied to account for residual effects, and half this correction is assigned as a systematic error.

It has been checked that the statistical correlation between the $D^{*0} \to D^0\pi^0$ signals in the $\Delta m(D^0, \pi^0)$ and $\Delta m(D^0, \gamma)$ distributions is negligible. Also, there is only a negligible fraction of cases where both photons from a $D^{*0} \to D^0\pi^0$ decay lead to an entry in the $\Delta m(D^0, \gamma)$ distribution.

4.4.4 Uncertainties from the b subtraction and the extrapolation

Subtraction of the $b \to D^{*0}$ contribution:
As mentioned in Sect. 4.1, it is assumed that the production of D^{*0} and D^{*+} mesons in b hadron decays is equal for scaled energies x_{D^0}>0.3. The error on the production of D^{*+} mesons in $Z^0 \to b\bar{b}$ decays as given in

equation (5) is taken into account. In addition, the production of D^{*0} mesons in $\overline{B}^0$ and B^- meson decays is varied within the range of the CLEO measurement given in equation (4) to assess the systematic error due to this assumption. At LEP, $\overline{B}^0$ and B^- mesons account for $(75.6 \pm 4.4)\%$ of all weakly decaying b hadrons [20]. To evaluate the production of D^{*0} mesons in decays of other bottom hadrons, the world average of $Br(\overline{B}^0$ or $B^- \to D^{*+}X) = (23.1 \pm 3.3)\%$ [20] is compared with the recent OPAL measurement of $R_b f(b \to D^{*+}) Br(D^{*+} \to D^0\pi^+) Br(D^0 \to K^-\pi^+) = (1.334 \pm 0.049 \pm 0.078) \times 10^{-3}$ [9]. From the branching fractions as given in [20], the production of D^{*+} mesons in $\overline{B}_s^0$ and Λ_b decays is then found to be $Br(\overline{B}_s^0$ or $\Lambda_b \to D^{*+}X) = 0.25 \pm 0.13$. Assuming equal D^{*0} and D^{*+} production in $\overline{B}_s^0$ and Λ_b decays, this leads to $R_b f(b \to \overline{B}_s^0$ or $\Lambda_b \to D^{*0}X) = 0.013$. A 100% error is assigned to this quantity.

Extrapolation to $x_{D^0} = 0$:
The extrapolation of the measured quantity $R_c\, f(c \to D^{*0})\, Br(D^0 \to K^-\pi^+)\big|_{x_{D^0}>0.3}$ from $x_{D^0}>0.3$ to the full range of scaled energies is based on the fragmentation function of Peterson et al. [15]. To assess the uncertainty associated with this extrapolation, it is repeated with mean scaled energies of D^{*0} mesons from $Z^0 \to c\bar{c}$ decays varied in the range given in Sect. 4.4.1. The difference from the previous result is interpreted as a systematic error.

4.5 Results of the D^{*0} measurement

The production of D^{*0} mesons in $Z^0 \to c\bar{c}$ events is measured to be

$$\begin{aligned} &R_c\, f(c \to D^{*0})\, Br(D^0 \to K^-\pi^+) \\ &= (1.44 \pm 0.36\,(stat.) \pm 0.30\,(syst.)) \times 10^{-3}\,. \end{aligned} \tag{9}$$

From this value, from the branching fraction $Br(D^0 \to K^-\pi^+) = (3.83 \pm 0.12)\%$ [20], and from the standard model prediction of $R_c = 0.172$ [24], the hadronisation fraction $f(c \to D^{*0})$ is computed to be

$$\begin{aligned} &f(c \to D^{*0}) \\ &= 0.218 \pm 0.054\,(stat.) \pm 0.045\,(syst.) \pm 0.007\,(ext.). \end{aligned} \tag{10}$$

Here, the last error corresponds to the error on the D^0 branching fraction.

5 Measurement of D_s^{*+} production

The decays of D_s^{*+} mesons are very simliar to those of D^{*0} mesons. The techniques developed for the D^{*0} analysis can therefore be used for the reconstruction of D_s^{*+} mesons.

The D_s^{*+} meson decays dominantly to the $D_s^+\gamma$ final state, since the $D_s^+\pi^0$ channel is suppressed by isospin invariance: $Br(D_s^{*+} \to D_s^+\pi^0)/Br(D_s^{*+} \to D_s^+\gamma) = 0.062^{+0.020}_{-0.018} \pm 0.022$ [25]. Thus, for the measurement of the production rate, only the $D_s^{*+} \to D_s^+\gamma$ decay is used.

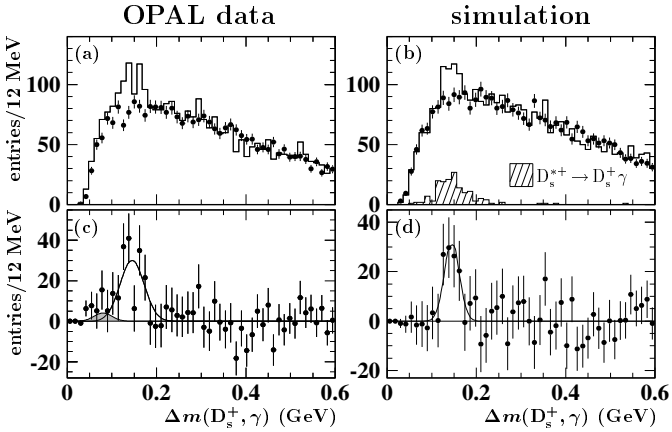

Fig. 4a–d. The mass difference distribution for the decay $D_s^{*+} \to D_s^+\gamma$. As before, in **a** and **b** the solid histogram corresponds to the signal sample, and points with error bars to the background sample. The signal contribution in the simulation is indicated by the hatched histogram.
The corresponding background subtracted distributions are shown in **c** and **d** together with the fitted signal parametrisation. The shaded Gaussian in figure **c** shows the expected contribution from $D_s^{*+} \to D_s^+\pi^0$ decays which is fixed in the fit

The D_s^+ mesons are reconstructed in their decay chain $D_s^+ \to \phi\pi^+$, $\phi \to K^+K^-$. Candidates with invariant masses $m_\phi < 1.05$ GeV and $1.90\ \text{GeV} < m_{D_s^+} < 2.04$ GeV, a scaled energy of $x_{D_s^+} > 0.35$, and a helicity angle of the pion in the D_s^+ rest frame satisfying $-0.90 < \cos\theta^* < 0.95$ are retained if the dE/dx requirements stated in Sect. 3.1 are fulfilled for the kaon and pion candidate tracks. The preselection of photons is identical to that described in Sect. 3.1.

The D_s^{*+} candidates are selected with a cut on a likelihood using the variables described in Sect. 3.1 accordingly, and taking the reconstructed mass of the ϕ and the cosine of the angle between the D_s^+ and one of the kaons in the ϕ rest frame as additional inputs. The background shape is determined from candidates in sidebands of m_ϕ and $m_{D_s^+}$ using the technique described in Sect. 3.2. The resulting mass difference distribution is shown in Fig. 4.

No attempt is made to separate the contributions from the processes $c \to D_s^{*+}$ and $b \to D_s^{*+}$. However, the efficiencies for D_s^{*+} reconstruction in $Z^0 \to c\bar{c}$ and $Z^0 \to b\bar{b}$ events have been found to be equal within errors. Thus, it is still reasonable to extract the overall D_s^{*+} production in Z^0 decays from a fit to the $\Delta m(D_s^+,\gamma)$ distribution. No isospin violating decays $D_s^{*+} \to D_s^+\pi^0$ have been generated in the simulation; in the data, a small contribution from such decays is expected at Δm values below the nominal D_s^{*+}–D_s^+ mass difference as shown in Fig. 4c. A double Gaussian is used to parametrise the signal, where the Gaussian at lower Δm is fixed to the expectation and varied by $\pm 100\%$ in case of the data. The number of D_s^{*+} mesons per hadronic Z^0 decay with $x_{D_s^+} > 0.35$ is found to be

$$\begin{aligned} &\bar{n}(Z^0 \to D_s^{*+})\, Br(D_s^{*+} \to D_s^+\gamma) \\ &Br(D_s^+ \to \phi\pi^+)\, Br(\phi \to K^+K^-)\big|_{x_{D_s^+}>0.35} \end{aligned}$$

Table 4. A breakdown of the relative statistical and dominant systematic errors on the D_s^{*+} measurement. The errors in brackets apply only when considering the value which has been extrapolated to all scaled energies $x_{D_s^+}$

relative statistical error	27.4%
relative systematic errors:	
extrapolation to $x_{D_s^+}=0$	(19.6%)
background shape	11.8%
tracking resolution	8.5%
D_s^+ lifetime	8.5%
effective shower isolation	8.1%
shower fit	6.9%
dE/dx preselection cuts	6.4%
$\langle x(X_b)\rangle_{Z^0\to b\bar{b}\to X_b}$	6.2%
others (evaluation similar to the D^{*0})	9.5%
total relative systematic error	23.8% (30.8%)

$$= (7.1 \pm 1.9 \pm 1.7) \times 10^{-4}\,, \qquad (11)$$

where the first error is statistical and the second systematic. The fit to the data has a χ^2 of 37.1 for 43 degrees of freedom.

The contributions to the systematic error were evaluated in a similar way as described earlier. Table 4 lists the most important errors. The largest systematic error on the value in (11) is introduced from the uncertainty in the background shape. The background sample is taken from a sideband in m_ϕ, and a correction has to be applied to account for the fact that fewer correctly reconstructed $\phi \to K^+K^-$ decays enter the background than the signal sample. When the fit is repeated with the same signal parametrisation plus an exponential to account for potential problems in the modelling of this bias, a consistent result is found. The deviation from the previous result is interpreted as systematic error. No other sources have been identified that could lead to a significant bias in the background shape.

The above D_s^{*+} measurement is extrapolated to the full range of scaled energies $x_{D_s^+}$. Here, a large systematic uncertainty is introduced from the unknown relative contribution from $c \to D_s^{*+}$ and $b \to D_s^{*+}$ components. When varying the unknown ratio $f(b\to D_s^{*+})/f(b\to D_s^+)$ within 0.6 ± 0.2, one finds the total rate

$$\begin{aligned} &\bar{n}(Z^0 \to D_s^{*+})\, Br(D_s^{*+} \to D_s^+\gamma) \\ &\times Br(D_s^+ \to \phi\pi^+)\, Br(\phi \to K^+K^-) \\ &= (1.69 \pm 0.46 \pm 0.40 \pm 0.33) \times 10^{-3}\,, \end{aligned} \qquad (12)$$

where the third error is introduced from the extrapolation to the full range of scaled energies. This rate is consistent with expectations and can be regarded as a further cross-check of the D^{*0} analysis, which uses very similar techniques.

6 The relative production rate of charmed vector mesons in $Z^0 \to c\bar{c}$ decays

The relative production rate of vector mesons containing the primary quark, P_V, is an important parameter in fragmentation and hadronisation models. Hadrons that contain the primary quark can in principle be produced either directly or in decays of higher resonances. Therefore, there are two possible definitions of P_V: the quantity $P_V^{\rm eff}$, where inclusive production (including decays of higher resonances) is considered, and $P_V^{\rm prim}$, which is defined when considering direct production only. These two values may differ due to the effects of decays of higher resonances, where some decays are forbidden by spin and parity conservation.

In previous investigations of P_V in the charm system [3–5], isospin invariance between the neutral and charged non-strange vector mesons was assumed. Given the measurement of the hadronisation fraction $f(c\to D^{*0})$ presented in the first part of this paper, an explicit check of this assumption is now possible.

Recently, a measurement of the spin alignment of D^{*+} mesons in $Z^0 \to c\bar{c}$ decays has been presented [23]. While P_V denotes the relative production of vector and pseudoscalar mesons, spin alignment measurements provide information on the relative production of different vector meson spin states. Thus, the combination of these two measurements provides further insight into the inclusive production of charmed mesons in the fragmentation process [3].

In the first part of this section, the existing OPAL measurements of the production of charmed mesons with no orbital angular momentum are used to derive a value of $P_V^{\rm eff}$, which is interpreted in conjunction with the D^{*+} spin alignment.

In the second part, additional input from excited D states is used to derive $P_V^{\rm prim}$. This quantity can be compared more directly to model calculations, since such models generally make predictions for primary hadron production. However, a determination of $P_V^{\rm prim}$ is experimentally challenging because of the difficulties in assessing the fraction of hadrons produced in decays of higher resonances. In this paper, the production of L=1 mesons is taken into account, while production and decay of higher states is considered a part of the fragmentation process. For each of the light flavours u, d, and s, four charmed mesons with orbital angular momentum L=1 are predicted. The naming convention is $D_J^{(*)}$, where J denotes the total spin of the meson, and an asterisk indicates that the meson has parity $(-1)^J$. In the following, these are collectively referred to as D^{**} mesons. Using the recent OPAL measurements of the hadronisation fractions $f(c\to D_1^0)$, $f(c\to D_2^{*0})$, and $f(c\to D_{s1}^+)$ [10], decays of D^{**} mesons can be taken into account to study the $P_V^{\rm prim}$ ratio. First, the dependence of $P_V^{\rm prim}$ on the production of the unmeasured L=1 resonances is discussed, and a model independent formula for the calculation of $P_V^{\rm prim}$ is derived. Second, the production

of the unmeasured L=1 resonances is assessed in a simple spin counting picture.

The following discussions are based on the $f(c \to D^{*0})$ measurement described in the first part of this paper and on previous OPAL measurements of charmed meson hadronisation fractions. Table 5 contains an overview of the values entering the following computations.

6.1 Tests of isospin invariance

Isospin invariance suggests equal primary production rates for corresponding $c\bar{u}$ and $c\bar{d}$ mesons. Thus, the hadronisation fractions $f(c \to D^{*0})$ and $f(c \to D^{*+})$ are expected to be the same, as long as decays of higher resonances contribute equally to both D^{*0} and D^{*+} production. For the vector mesons D^{*0} and D^{*+}, isospin invariance can therefore be tested directly from the D^{*0} and D^{*+} production rate measurements and the branching fraction $Br(D^{*+} \to D^0\pi^+)$ as listed in Table 5, resulting in a ratio of

$$\frac{f(c \to D^{*0})}{f(c \to D^{*+})} = 0.94 \pm 0.31\,, \tag{13}$$

consistent with 1. As mentioned in Sect. 4.1, the $c \to D^{*0}$ measurement assumes equal production of D^{*0} and D^{*+} mesons in b hadron decays as justified by the CLEO result given in (4). The error on the CLEO measurement is treated as a systematic uncertainty on $f(c \to D^{*0})$ as discussed in Sect. 4.4.4, and it can be seen from Table 3 that this systematic error is substantially smaller than the statistical error on $f(c \to D^{*0})$.

Since $D^{*0} \to D^+\pi^-$ decays are kinematically forbidden while $D^{*+} \to D^0\pi^+$ decays are not, the observed hadronisation fractions of D^0 and D^+ mesons are expected to differ even if the primary production rates are equal. When taking into account these D^{*+} decays and assuming isospin invariance between D^0 and D^+ mesons, the ratio

$$R \equiv \frac{f(c \to D^0) - f(c \to D^+)}{f(c \to D^{*0}) + \left(2Br(D^{*+} \to D^0\pi^+) - 1\right) f(c \to D^{*+})} \tag{14}$$

is expected to be equal to one. From the values given in Table 5, one obtains $R = 1.19 \pm 0.36$, consistent with 1. Under the assumption of equal hadronisation fractions $f(c \to D^{*0}) = f(c \to D^{*+})$, other experiments [4] have obtained values consistent with this result.

With isospin invariance thus confirmed within experimental errors, the hadronisation fractions of D^{*0} and D^{*+} mesons are assumed to be equal in the following. The mean $D^{*0/+}$ hadronisation fraction is then defined as the weighted average of the values of $f(c \to D^{*0/+})$ determined from (14) and from the direct measurements of $f(c \to D^{*0})$ and $f(c \to D^{*+})$. The resulting value of

$$\begin{aligned} &R_c\, f(c \to D^{*0/+})\, Br(D^{*+} \to D^0\pi^+)\, Br(D^0 \to K^-\pi^+) \\ &= (1.045 \pm 0.044) \times 10^{-3} \end{aligned} \tag{15}$$

is used in the computation of P_V in the following sections.

6.2 Effective charmed meson production

The effective value $P_V^{\rm eff}$ is calculated from the mean $D^{*0/+}$ hadronisation fraction derived in the previous section and the measurements listed in Table 5 to be

$$P_V^{\rm eff} = \frac{2f(c \to D^{*0/+})}{f(c \to D^0) + f(c \to D^+)} = 0.57 \pm 0.05\,. \tag{16}$$

Here, the assumption has been made that isospin invariance is valid, as tested in the previous section. If, instead, the measured hadronisation fractions are directly combined without the assumption of isospin invariance for D^{*0} and D^{*+} production, a value of $P_V^{\rm eff} = \frac{f(c \to D^{*0}) + f(c \to D^{*+})}{f(c \to D^0) + f(c \to D^+)} = 0.55 \pm 0.10$ is obtained. In principle, the measurements are expected to be correlated. The largest correlation is expected between $f(c \to D^0)$ and $f(c \to D^{*+})$ and has been estimated to be smaller than 30%. A shift on $P_V^{\rm eff}$ of less than 0.01 is introduced by the correction.

The result from (16) can be interpreted in connection with the D^* spin alignment. In the fragmentation process, four different spin states of charmed mesons without orbital excitation can be formed: The vector mesons D^{*0}, D^{*+}, and D_s^{*+} with states $J = 1$ and $m = -1, 0, +1$, as well as the pseudoscalar mesons D^0, D^+, and D_s^+ with $J = m = 0$. The relative inclusive production probabilities $\mathcal{P}$ for these states are related to $P_V^{\rm eff}$ and to the spin density matrix element ρ_{00} of D^* mesons from $Z^0 \to c\bar{c}$ events via [3,29]

$$\begin{aligned} P_V^{\rm eff} &= \mathcal{P}_{J=1}^{m=0} + \mathcal{P}_{J=1}^{m=\pm1} \quad \text{and} \\ \rho_{00} &= \mathcal{P}_{J=1}^{m=0} / (\mathcal{P}_{J=1}^{m=0} + \mathcal{P}_{J=1}^{m=\pm1})\,. \end{aligned} \tag{17}$$

Here, $\mathcal{P}_{J=1}^{m=\pm1}$ denotes the sum of the production probabilities for the $m = +1$ and $m = -1$ states that cannot be distinguished experimentally. The spin density matrix element ρ_{00} gives the probability to find a vector meson in the $m = 0$ state. A simple spin counting model suggests values of $\mathcal{P}_{J=1}^{m=\pm1} = \frac{1}{2}$ and $\mathcal{P}_{J=1}^{m=0} = \mathcal{P}_{J=0}^{m=0} = \frac{1}{4}$ (see for instance [29]).

For D^{*+} mesons from $Z^0 \to c\bar{c}$ decays with scaled energies $x_{D^{*+}} > 0.2$, ρ_{00} has been measured at OPAL to be $\rho_{00} = 0.40 \pm 0.02$ [23]. From this result and the above value of $P_V^{\rm eff}$, the production probabilities

$$\begin{aligned} \mathcal{P}_{J=1}^{m=0} &= \rho_{00} P_V^{\rm eff} = 0.23 \pm 0.02\,, \\ \mathcal{P}_{J=1}^{m=\pm1} &= (1 - \rho_{00}) P_V^{\rm eff} = 0.34 \pm 0.03\,, \quad \text{and} \\ \mathcal{P}_{J=0}^{m=0} &= 1 - P_V^{\rm eff} = 0.43 \pm 0.05 \end{aligned} \tag{18}$$

can be derived, where it has been assumed that the measured spin density matrix element ρ_{00} applies to both D^{*0} and D^{*+} mesons in $Z^0 \to c\bar{c}$ events.

These probabilities show a clear deviation from the simple spin counting picture. The production of vector mesons is suppressed in favour of pseudoscalar mesons. This is mostly due to a suppression of the m=±1 vector states, while the production of the J=1, m=0 state agrees within errors with a spin counting picture.

An overall suppression of vector meson production is, for instance, expected in thermodynamic models, where

Table 5. The measurements and assumptions entering the computation of P_V values

charmed meson production, OPAL measurements	value and reference
$R_c\ f(c\to D^{*0})\ Br(D^0\to K^-\pi^+)$	$(1.44\pm0.36\pm0.30)\times10^{-3}$ (Sect. 4.5)
$R_c\ f(c\to D^{*+})\ Br(D^{*+}\to D^0\pi^+)\,Br(D^0\to K^-\pi^+)$	$(1.041\pm0.020\pm0.040)\times10^{-3}$ [9]
$R_c\ f(c\to D^0)\ Br(D^0\to K^-\pi^+)$	$(0.389\pm0.027^{+0.026}_{-0.024})\times10^{-2}$ [8]
$R_c\ f(c\to D^+)\ Br(D^+\to K^-\pi^+\pi^+)$	$(0.358\pm0.046^{+0.025}_{-0.031})\times10^{-2}$ [8]
$R_c\ f(c\to D_1^0$ or $D_2^{*0})\ Br(D_1^0$ or $D_2^{*0}\to D^{*+}\pi^-)$	$(4.2\pm1.1^{+0.5+0.2}_{-0.7-0.3})\times10^{-3}$ [10]
$\frac{f(c\to D_1^0\to D^{*+}\pi^-)}{f(c\to D_1^0\to D^{*+}\pi^-)+f(c\to D_2^{*0}\to D^{*+}\pi^-)}$	$0.56\pm0.15^{+0.03}_{-0.04}$ [10]
$R_c\ f(c\to D_{s1}^+)$	$(2.8^{+0.8}_{-0.7}\pm0.3\pm0.4)\times10^{-3}$ [10]
branching fractions and ratios	value and reference
$Br(D^0\to K^-\pi^+)$	0.0383 ± 0.0012 [20]
$Br(D^+\to K^-\pi^+\pi^+)/Br(D^0\to K^-\pi^+)$	$2.35\pm0.16\pm0.16$ [26]
$Br(D^{*+}\to D^0\pi^+)$	0.683 ± 0.014 [20]
$\frac{Br(D_2^*\to D^*\pi)}{Br(D_2^*\to D^*\pi)+Br(D_2^*\to D\pi)}\approx Br(D_2^*\to D^*\pi)$	0.311 ± 0.051 [20]
$\frac{Br(D_{s2}^{*+}\to D^*K)}{Br(D_{s2}^{*+}\to D^*K)+Br(D_{s2}^{*+}\to DK)}\approx Br(D_{s2}^{*+}\to D^*K)$	0.107 ± 0.016 [10,27,28]
assumption on relative D^{**} meson production in a spin counting model	
$f(c\to D_0^{*0}):f(c\to D_1'^0):f(c\to D_1^0):f(c\to D_2^{*0})$ $f(c\to D_{s0}^{*+}):f(c\to D_{s1}'^+):f(c\to D_{s1}^+):f(c\to D_{s2}^{*+})$	$1:3:3:5$

the constituents of hadrons are pictured as a gas with a temperature T, such that a relative suppression of the heavier states by a factor of $\exp(-\Delta m/T)$ is predicted. From the above value of $P_V^{\rm eff}$, the temperature is calculated to be $T=\left(174^{+62}_{-36}\right)$ MeV, consistent with the value determined in [30]. It should be noted, however, that thermodynamic models fail to explain the observed non-zero spin alignment.

6.3 Primary charmed meson production

For the determination of $P_V^{\rm prim}$, the effects of the decays of L=1 charmed mesons have to be taken into account. The hadronisation fractions $f(c\to D_1^0)$, $f(c\to D_2^{*0})$, and $f(c\to D_{s1}^+)$ have been measured at LEP, whereas the production of the broad resonances D_0^* and D_1' has not yet been measured. Since the charged D^{**+} mesons have not yet been observed in Z^0 decays, isospin invariance is assumed to be valid in charm fragmentation to assess the production of these resonances, which implies equal hadronisation fractions for corresponding D^{**+} and D^{**0} states. Furthermore, it is assumed in the following that for D^{**} mesons, the relative production of the different spin states does not depend on the light quark flavour.

The ratio $P_V^{\rm prim}$ can be expressed as a function of two unmeasured hadronisation fractions, $f(c\to D_0^{*0})$ and $f(c\to D_1'^0)$, and two known parameters A and B which depend on the measurements listed in Table 5:

$$P_V^{\rm prim}=\frac{A-R_c f(c\to D_1'^0)}{B-R_c\left[f(c\to D_0^{*0})+f(c\to D_1'^0)\right]}\,. \qquad (19)$$

The complete derivation and the exact formulae for A and B are given in appendix A. The parameters A and B are found to be

$$A=(2.29\pm0.34)\times10^{-2}\ \text{and}\quad B=(3.82\pm0.89)\times10^{-2}\,, \qquad (20)$$

with a positive correlation between A and B of 77%.

In Fig. 5a–c, the results for $P_V^{\rm prim}$ are shown as a function of the two unknown hadronisation fractions. In general, low values of $P_V^{\rm prim}$ are obtained for small D_0^* and large D_1' production and vice versa. This analysis shows that the value of $P_V^{\rm prim}$ is not very sensitive to the production of the unmeasured broad D^{**} resonances. Generally, the range of $P_V^{\rm prim}$ values is consistent with predictions. However, to test a given model, a clearer statement can be made when following the procedure outlined below.

In contrast to the above discussion, a test of any specific fragmentation model can be performed when using its prediction for the relative primary production of the different L=0 and L=1 states. While the prediction for the L=0 states is directly equivalent to a prediction of $P_V^{\rm prim}$, the model prediction in the L=1 sector provides information on the production of the unmeasured L=1 resonances, which can in turn be used in conjunction with the measured hadronisation fractions to obtain an experimental value of $P_V^{\rm prim}$. Such a test is described in the following for the simplest case, a spin counting model.

A spin counting model predicts the relative primary production of D and D^* mesons to be 1 : 3. At the same time, for D^{**} mesons, the relative production of the D_0^* : D_1' : D_1 : D_2^* resonances is predicted to be 1 : 3 : 3 : 5. When using the latter prediction, $P_V^{\rm prim}$ is found to be

$$P_V^{\rm prim}(\text{spin counting for } D^{**})=0.55\pm0.08\,. \qquad (21)$$

However, since the validity of spin counting was assumed in the calculation, the value of $P_V^{\rm prim}$ is fixed and should be 0.75. Thus, from the discrepancy between the above

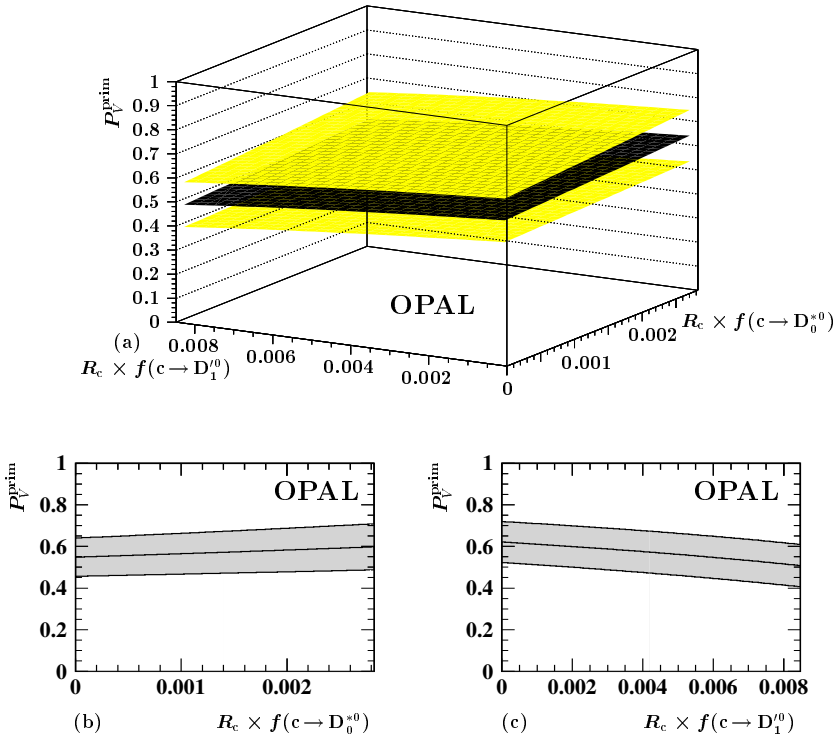

Fig. 5a–c. The dependence of $P_V^{\rm prim}$ on the two unmeasured multiplicities $R_c \times f(c \to D_0^{*0})$ and $R_c \times f(c \to D_1'^0)$ is shown in **a**. Each of these quantities is varied between 0 and twice the value as expected from a spin counting picture. Plots **b** and **c** show the dependence on each one of these multiplicities when the other is fixed at the spin counting expectation. The error contours correspond to one standard deviation. They include the experimental error on the relative production of D_1^0 and D_2^{*0} mesons as measured in [10]

value and 0.75, the simultanous description of both L=0 and L=1 charmed meson production in a spin counting picture is disfavoured by 2.7 standard deviations. Within the framework of this model test, the relative production of the four D^{**} spin states need not be taken from experiment, since it is predicted by the model. Thus, the experimental error on the model test is reduced as compared to the model independent values shown in Fig. 5a–c. As mentioned above, the value in (21) is part of a consistency check of a specific model and should not be interpreted as a stand-alone measurement.

In principle, a comparison of the hadronisation fractions $f(c \to D_s^{*+})$ and $f(c \to D_s^+)$ yields a model independent measurement of $P_V^{\rm prim}$. However, the result from Sect. 5 cannot be interpreted in terms of vector and pseudoscalar meson production in charm hadronisation, since no information on the separation of the $c \to D_s^{*+}$ and $b \to D_s^{*+}$ components exists.

7 Summary and conclusion

A first measurement of the hadronisation fraction $f(c \to D^{*0})$ in $Z^0 \to c\bar{c}$ decays is presented:

$$f(c \to D^{*0}) = 0.218 \pm 0.054\,(stat.) \pm 0.045\,(syst.) \pm 0.007\,(ext.)\,.$$

This result is consistent with the expectation from isospin invariance. The production rate of D_s^{*+} mesons in hadronic Z^0 decays has been measured for the first time:

$$\bar{n}(Z^0 \to D_s^{*+})\, Br(D_s^{*+} \to D_s^+ \gamma) \times Br(D_s^+ \to \phi\pi^+)\, Br(\phi \to K^+K^-) = (1.69 \pm 0.46\,(stat.) \pm 0.52\,(syst.)) \times 10^{-3}\,.$$

The relative production of vector charmed mesons in $Z^0 \to c\bar{c}$ events, P_V, is evaluated both considering inclusive production ($P_V^{\rm eff}$) and taking into account the effects of secondary production in D^{**} decays ($P_V^{\rm prim}$). A value of

$$P_V^{\rm eff} = 0.57 \pm 0.05$$

has been derived from OPAL measurements, consistent with previous results. The dependence of $P_V^{\rm prim}$ on the unmeasured D^{**} multiplicities is determined in a model independent calculation, where a weak dependence on the production of the unmeasured broad D^{**} resonances has been found. From the determination of $P_V^{\rm prim}$, it is found that for the description of the production of charmed mesons in $Z^0 \to c\bar{c}$ decays, a simple spin counting picture is disfavoured by 2.7 standard deviations.

Acknowledgements. We particularly wish to thank the SL Division for the efficient operation of the LEP accelerator at all energies and for their continuing close cooperation with our experimental group. We thank our colleagues from CEA, DAPNIA/SPP, CE-Saclay for their efforts over the years on the time-of-flight and trigger systems which we continue to use. In addition to the support staff at our own institutions we are pleased to acknowledge the
Department of Energy, USA,
National Science Foundation, USA,
Particle Physics and Astronomy Research Council, UK,
Natural Sciences and Engineering Research Council, Canada,
Israel Science Foundation, administered by the Israel Academy of Science and Humanities,
Minerva Gesellschaft,

Table 6. Properties of the neutral, non-strange excited D mesons. For the decay channels, the same restrictions as shown here apply to D^{**+} and D_s^{**+} mesons, where in the case of D_s^{**+} decays, pions have to be replaced by kaons

name	D_0^{*0}	$D_1'^0$	D_1^0	D_2^{*0}
$j = s_q + L$	$(1/2)^+$		$(3/2)^+$	
decay	S-wave		D-wave	
spin-parity J^P	0^+	1^+	1^+	2^+
decay channels	$D\pi$	$D^*\pi$	$D^*\pi$	$D\pi$, $D^*\pi$
width (MeV) [20]	~ 100	~ 100	$18.9 \pm^{4.6}_{3.5}$	23 ± 5
mass (MeV) [20]	(not observed)		2422.2 ± 1.8	2458.9 ± 2.0

Benoziyo Center for High Energy Physics,
Japanese Ministry of Education, Science and Culture (the Monbusho) and a grant under the Monbusho International Science Research Program,
German Israeli Bi-national Science Foundation (GIF),
Bundesministerium für Bildung, Wissenschaft, Forschung und Technologie, Germany,
National Research Council of Canada,
Research Corporation, USA,
Hungarian Foundation for Scientific Research, OTKA T-016660, T023793 and OTKA F-023259.

A Model independent calculation of $P_V^{\rm prim}$

In this appendix, details of the calculations that lead to the dependence of the model independent value of $P_V^{\rm prim}$ on the production of the broad L=1 charmed mesons (Eq. (19)) are provided.

As discussed in the text, the contributions from decays of D^{**} mesons have to be taken into account when calculating $P_V^{\rm prim}$. Two assumptions are made on D^{**} production:

- Since D^{**+} mesons have not yet been observed in $Z^0 \to c\bar{c}$ decays, isospin invariance is assumed to be valid which yields equal production rates for corresponding D^{**0} and D^{**+} spin states.
- For each light quark flavour q=u,d,s, two broad and two narrow L=1 $c\bar{q}$ mesons are predicted. For the $c\bar{u}$ system, both narrow resonances (D_1^0 and D_2^{*0}) have been measured at OPAL, whereas only one narrow $c\bar{s}$ resonance (D_{s1}^+) has been measured. Thus, the additional assumption is made that the relative production of the different L=1 spin states does not depend on the flavour of the light quark.

Under these two assumptions, the production of any L=1 charmed meson can be expressed in terms of measured rates and two unknown parameters, $f(c \to D_0^{*0})$ and $f(c \to D_1'^0)$.

The OPAL D_{s1}^+ production measurement [10] assumes a 100% branching for $D_{s1}^+ \to D^{(*)}K$ decays (i. e. to non-strange, charmed non-orbitally excited mesons). Therefore, any contribution from $D_s^{**+} \to D_s^{(*)+}X$ decays is implicitly taken into account when using the measured D_{s1}^+ multiplicity for an evaluation of $P_V^{\rm prim}$.

The quantity $P_V^{\rm prim}$ is calculated as follows:

$$P_V^{\rm prim} = \frac{V^{\rm prim}}{V^{\rm prim} + P^{\rm prim}} \tag{22}$$

$$= \frac{V^{\rm eff} - \left(T_{(s)} \to V\right)}{(V+P)^{\rm eff} - \left(T_{(s)} \to V \text{ or } P\right)} \ , \tag{23}$$

where in the above formula, V and P stand for non-strange charmed vector and pseudoscalar mesons, respectively, whereas $T_{(s)}$ denotes the sum of non-strange and strange charmed tensor mesons (D^{**} and D_s^{**}). Thus,

$$P_V^{\rm prim} = \frac{2f(c\to D^{*+}) - 2f(c\to D^{**0}\to D^{*0/+}) - f(c\to D_s^{**+}\to D^{*0/+})}{f(c\to D^0)+f(c\to D^+) - 2f(c\to D^{**0}) - f(c\to D_s^{**+})} \tag{24}$$

where the factors of 2 are introduced from the assumptions $f(c \to D^{*0}) = f(c \to D^{*+})$ and $f(c \to D^{**0}) = f(c \to D^{**+})$.

The symbol $f(c \to D^{**} \to D^{*0/+})$ is a shorthand notation for the hadronisation fraction of a charmed quark to a D^{**} meson times the fraction of D^{**} mesons decaying to a $D^{*0/+}$. Spin and parity conservation restrict the possible decays of the different D^{**} spin states, as is illustrated in Table 6, where a summary of predictions and measurements [20] for the four D^{**0} spin states is given. Thus, the fraction of D^{**} mesons decaying to a $D^{*0/+}$ depends both on the relative production of the different D^{**} spin states and on the branching ratio $Br(D_2^* \to D^{*0/+})$, since for the D_2^* resonance, decays to both D^* and D are allowed. Due to phase-space effects, the branching fraction $Br_s^{**} \equiv Br(D_{s2}^{*+} \to D^{*0/+})$ of D_{s2}^{*+} mesons to a D^{*0} or D^{*+} is expected to differ from the corresponding quantity $Br^{**} \equiv Br(D_2^{*0} \to D^{*0/+})$ for non-strange D^{**} mesons, see Table 5.

Using the shorthand notation $f_{D_X} \equiv f(c \to D_X)$, (19) can then be derived as follows:

$$P_V^{\rm prim} = \frac{2f_{D^*} - 2\left(f_{D_1'^0} + f_{D_1^0} + Br^{**} f_{D_2^{*0}}\right) - \frac{f_{D_{s1}^+}}{f_{D_1^0}}\left(f_{D_1'^0} + f_{D_1^0} + Br_s^{**} f_{D_2^{*0}}\right)}{f_{D^0} + f_{D^+} - 2\left(f_{D_0^{*0}} + f_{D_1'^0} + f_{D_1^0} + f_{D_2^{*0}}\right) - \frac{f_{D_{s1}^+}}{f_{D_1^0}}\left(f_{D_0^{*0}} + f_{D_1'^0} + f_{D_1^0} + f_{D_2^{*0}}\right)} =: \frac{A - R_c f_{D_1'^0}}{B - R_c\left(f_{D_1'^0} + f_{D_0^{*0}}\right)} \ , \tag{25}$$

where in the transition to the third line, both numerator and denominator are multiplied by a factor of

$R_c / \left(2 + \frac{f(c \to D_s^{**+})}{f(c \to D^{**0})}\right)$. The parameters A and B are then given by

$$\begin{aligned} A = R_c \Big[& 2\, f(c \to D^{*0/+}) - 2 \big(f(c \to D_1^0) \\ & + f(c \to D_2^{*0} \to D^{*0/+}) \big) \\ & - \Big(f(c \to D_{s1}^+) + f(c \to D_{s2}^{*+} \to D^{*0/+}) \Big) \Big] \\ & / \left[2 + \frac{f(c \to D_s^{**+})}{f(c \to D^{**0})} \right] \quad \text{and} \end{aligned} \tag{26}$$

$$\begin{aligned} B \equiv R_c \Big[& f(c \to D^0) + f(c \to D^+) \\ & - 2 \big(f(c \to D_1^0) + f(c \to D_2^{*0}) \big) \\ & - \frac{f(c \to D_s^{**+})}{f(c \to D^{**0})} \big(f(c \to D_{s1}^+) + f(c \to D_{s2}^{*+}) \big) \Big] \\ & / \left[2 + \frac{f(c \to D_s^{**+})}{f(c \to D^{**0})} \right], \end{aligned} \tag{27}$$

respectively.

References

1. K. Cheung, *Recent Progress on Perturbative QCD Fragmentation Functions,* Proceedings of the 1995 PASCOS/Hopkins Workshop, Baltimore, or hep-ph/**9505365**; E. Braaten, K. Cheung, S. Fleming, and T.C. Yuan, Phys. Rev. **D51** (1995) 4819; Y.-Q. Chen, Phys. Rev. **D48** (1993) 5181; M. Suzuki, Phys. Rev. **D33** (1986) 676; R. Suaya, J.S. Townsend, Phys. Rev. **D19** (1979) 1414.
2. OPAL Collaboration, K. Ackerstaff et al., Z. Phys. **C74** (1997) 413; ALEPH Collaboration, D. Buskulic et al., Z. Phys. **C69** (1996) 393; DELPHI Collaboration, P. Abreu et al., Z. Phys. **C68** (1995) 353; L3 Collaboration, M. Acciarri et al., Phys. Lett. **B345** (1995) 589.
3. M. Anselmino et al., *Quark Fragmentation into Vector and Pseudoscalar Mesons at LEP,* CERN-PPE/97-136, submitted to Phys. Lett. **B**.
4. ALEPH Collaboration, D. Buskulic et al., Z. Phys. **C62** (1994) 1; DELPHI Collaboration, P. Abreu et al., Z. Phys. **C59** (1993) 533, erratum-ibid. **C65** (1995) 709.
5. F. Fiedler, *Measurements of Hadronisation Aspects of Heavy Quark Production in* Z^0 *Decays,* to be published in the proceedings of the IVth International Workshop on Progress in Heavy Quark Physics, Rostock, Germany, September 20-22, 1997.
6. Yi-Jin Pei, Z. Phys. **C72** (1996) 39.
7. L3 Collaboration, M. Acciarri et al., Phys. Lett. **B396** (1997) 327.
8. OPAL Collaboration, G. Alexander et al., Z. Phys. **C72** (1996) 1.
9. OPAL Collaboration, K. Ackerstaff et al., Eur. Phys. J. **C1** (1998) 439
10. OPAL Collaboration, K. Ackerstaff et al., Z. Phys. **C76** (1997) 425
11. OPAL Collaboration, P.P. Allport et al., Nucl. Instr. and Meth. **A346** (1994) 476; OPAL Collaboration, P.P. Allport et al., Nucl. Instr. and Meth. **A324** (1993) 34; O. Biebel et al., Nucl. Instr. and Meth. **A323** (1992) 169; M. Hauschild et al., Nucl. Instr. and Meth. **A314** (1992) 74; OPAL Collaboration, K. Ahmet et al., Nucl. Instr. and Meth. **A305** (1991) 275.
12. OPAL Collaboration, G. Alexander et al., Z. Phys. **C52** (1991) 175.
13. T. Sjöstrand, Comp. Phys. Comm. **82** (1994) 74.
14. OPAL Collaboration, G. Alexander et al., Z. Phys. **C69** (1996) 543.
15. C. Peterson, D. Schlatter, I. Schmitt and P. M. Zerwas, Phys. Rev. **D27** (1983) 105.
16. J. Allison et al., Nucl. Instr. and Meth. **A317** (1992) 47.
17. M. Hauschild et al., Nucl. Instr. and Meth. **A314** (1992) 74.
18. OPAL Collaboration, R. Akers et al., Z. Phys. **C66** (1995), 19.
19. OPAL Collaboration, G. Alexander et al., Z. Phys. **C73** (1997) 587.
20. Particle Data Group, Phys. Rev. **D54** (1996) 1.
21. CLEO Collaboration, L. Gibbons et al., Phys. Rev. D **56** (1997) 3783
22. The LEP Collaborations ALEPH, DELPHI, L3, and OPAL, and the LEP Electroweak working group, *Combining Heavy Flavour Electroweak Measurements at LEP,* CERN-PPE/96-017 (1996).
23. OPAL Collaboration, K. Ackerstaff et al., Z. Phys. **C74** (1997) 437.
24. The LEP Collaborations ALEPH, DELPHI, L3, and OPAL, the LEP Electroweak working group, and the SLD Heavy Flavour Group, *A Combination of Preliminary Electroweak Measurements and Constraints on the Standard Model,* CERN-PPE/96-183 (1996).
25. CLEO Collaboration, J. Gronberg et al., Phys. Rev. Lett. **75** (1995) 3232.
26. CLEO Collaboration, R. Balest et al., Phys. Rev. Lett. **72** (1994) 2328.
27. S. Godfrey and R. Kokoski, Phys. Rev. **D43** (1991) 1679.
28. CLEO Collaboration, Y. Kubota et al., Phys. Rev. Lett. **72** (1994) 1972.
29. A. F. Falk and M. E. Peskin, Phys. Rev. **D49** (1994) 3320.
30. F. Becattini, *Universality of thermal hadron production in* pp, $p\bar{p}$ *and* e^+e^- *collisions,* hep-ph/9701275, v2, to be published in the proceedings of the XXXIII Eloisatron Workshop on Universality features in multihadron production and the leading effect, October 19-25 1996, Erice, Italy.